Construction of a three-dimensional rGO/CoFe$_2$O$_4$ nanorods composite with enhanced microwave absorption performance

Hanwen Zong[1], Haibo Yang[1],*, Jingjing Dong[1], Liang Ma[2], Ying Lin[1],*, Yun Qiu[1], and Bo Wen[1]

[1] Shaanxi Key Laboratory of Green Preparation and Functionalization for Inorganic Materials, School of Materials Science and Engineering, Shaanxi University of Science and Technology, Xi'an 710021, China
[2] Xianyang Non-metallic Mineral R & D Institute Co.,Ltd, Xianyang, China

ABSTRACT

Nowadays, designing and fabricating electromagnetic (EM) wave absorbers with lightweight and strong reflection loss (RL) is still urgent. Herein, rGO/CoFe$_2$O$_4$ composite combined with magnetic CoFe$_2$O$_4$ nanorods and reduced graphene oxide (rGO) was fabricated via molten salt method in combination with a simple etching route. The EM absorption ability of rGO/CoFe$_2$O$_4$ nanorods composite can be regulated by changing the rGO addition amount. Particularly, the absorber for rGO/CoFe$_2$O$_4$ nanorods composite with the rGO addition amount of 70 mg (S-70) displays favorable EM wave absorption properties. The optimal RL value is − 56.3 dB at the frequency of 16.9 GHz, when the corresponding thickness is 1.4 mm. The effective absorption bandwidth (EAB, RL < − 10 dB) is 4.3 GHz, when the thickness is 1.6 mm. Consequently, the rGO/CoFe$_2$O$_4$ nanorods composite is a potential candidate for microwave absorbing materials.

1 Introduction

Due to the widespread use of communication devices and radar technology, EM radiation has become a tricky pollution question in many fields. It even has been regarded as a serious threat to electronic stability, healthcare and military fields [1–3]. So, it brings the great demand for developing high-performance EM wave absorbers which possess strong absorption, wide absorption bandwidth, thin thickness and lightweight [4–6]. According to theoretical analysis and experimental verification, the EM absorption materials absorbing microwave energy is basically impacted by dielectric and/or magnetic loss [7–9]. However, materials with only one loss factor are hard to obtain excellent EM wave absorption properties owing to inappropriate impedance matching and limited loss mechanism [1, 10]. Therefore, through artificially adjusting the EM

Address correspondence to E-mail: yanghaibo@sust.edu.cn; linying_333@163.com

parameters, fabricating the magnetic/dielectric composites with strong absorption capacity, high efficiency and wide absorption frequency has become a credible strategy to obtain excellent EM wave absorbers [11–14].

rGO has drawn considerable attention owing to two-dimensional (2D) single-layer structure, large specific surface area, abundant residual defects and appropriate dielectric loss [15, 16], which may lead to excellent electrical conductivity, thermal and mechanical properties. Nevertheless, the EM wave absorption properties of rGO are very poor because its high electric conductivity and low magnetic permeability lead to impedance mismatching characteristic [17, 18]. Therefore, many researchers have reported that modifying rGO surface with magnetic components can moderate its impedance matching and improve the absorption of the EM wave [19, 20]. Zhang et al. investigated that ternary $rGO/MnFe_2O_4/PVDF$ composites exhibited enhanced EM wave absorption performance because of the synergetic effects between rGO, $MnFe_2O_4$, and PVDF [2]. Chen et al. presented a simple synthetic strategy for expanded graphite/polyaniline/$CoFe_2O_4$. The composite displays the best absorption of − 19.1 dB and a thickness of 0.5 mm [21]. Zhang et al. reported that combined $CoFe_2O_4$ with rGO can ameliorate EM wave adsorbing performances of the former, and the RL_{max} of composite is − 53.6 dB at 11.4 GHz [22]. Hence, introducing magnetic ferrites onto the surface of rGO sheets undoubtedly becomes a suitable strategy.

As a typical spinel ferrite, cobalt ferrite ($CoFe_2O_4$) has outstanding properties, such as moderate room-temperature saturation magnetization, high chemical stability and mechanical hardness [23], which makes it to be a promising candidate for microwave absorbers. Many efforts have been made to design $CoFe_2O_4$-based composites with controllable electromagnetic parameters. Li et al. successfully fabricated $CoFe_2O_4$/graphene oxide hybrids and obtained a maximum RL of − 10.8 dB at 4.0 mm with frequency of 9.2 GHz [24]. Zhang et al. prepared lightweight PANS@ $CoFe_2O_4$-RGO epoxy composites. The composites display the best absorption of − 14.8 dB at 13.6 GHz with a matching thickness of 2 mm [25]. Moitra et al. manufactured multifunctional $CoFe_2O_4$-reduced graphene oxide nanocomposites by a simple 'in situ' co-precipitation method and the RL_{max} of this nanocomposites is − 31.3 dB at

9.1 GHz [26]. Zhang et al. obtained porous rugby-shaped $CoFe_2O_4$ particles and obtained optimal RL of − 34.1 dB at the thickness of 2.5 mm and the EAB is 2.6 GHz [23]. Fu et al. prepared hollow $CoFe_2O_4$ sphere/graphene composites and studied their possible absorbing mechanism [27]. However, the density and thickness is still unsatisfied, which heavily restricts its practical application.

Herein, we synthesized a three-dimensional rGO/$CoFe_2O_4$ nanorods composite by using a facile-etching method. The corresponding synthetic route is displayed in Scheme 1. The hybrids show significant microwave absorption ability in terms of both the reflection loss and thickness because of moderate impedance matching of materials. Combining the two materials not only takes advantage of both but also increases the impedance matching and multiple interface loss between different materials [28]. Hence, this composite can be used as a potential lightweight microwave absorber.

2 Experimental section

2.1 Materials

Flake Graphite was provided by Qingdao Jinhui graphite Co. Ltd. Graphene oxide (GO) was prepared via Hummer's method with some modification. Iron nitrate nonahydrate ($Fe(NO_3)_3·9H_2O$), sodium chloride (NaCl), cobalt nitrate hexahydrate ($Co(NO_3)_2·6H_2O$), dimethyl formamide (DMF) and methyl mercaptoacetate ($C_3H_6O_2S$) were obtained from Sinopharm Chemical Reagent Co. Ltd. Hydrazine ($NH_2NH_2·H_2O$) was purchased from Aladdin Co. Ltd. All the chemicals were used without further purification.

2.2 Preparation of CoFe₂O₄ particles

$CoFe_2O_4$ particles were synthesized by molten salt method. According to the stoichiometry of $CoFe_2O_4$, the proper amount of $Fe(NO_3)_3·9H_2O$ and $Co(NO_3)_2·6H_2O$ were mixed in 50 mL ultrapure water and stirred for 2 h. The mixture were transferred into 100 mL kettle and heated at 180 °C for 12 h. A black precipitate of $CoFe_2O_4$ was obtained after 12 h. The precipitate was washed by centrifuge machine and dried by vacuum oven. Then, the
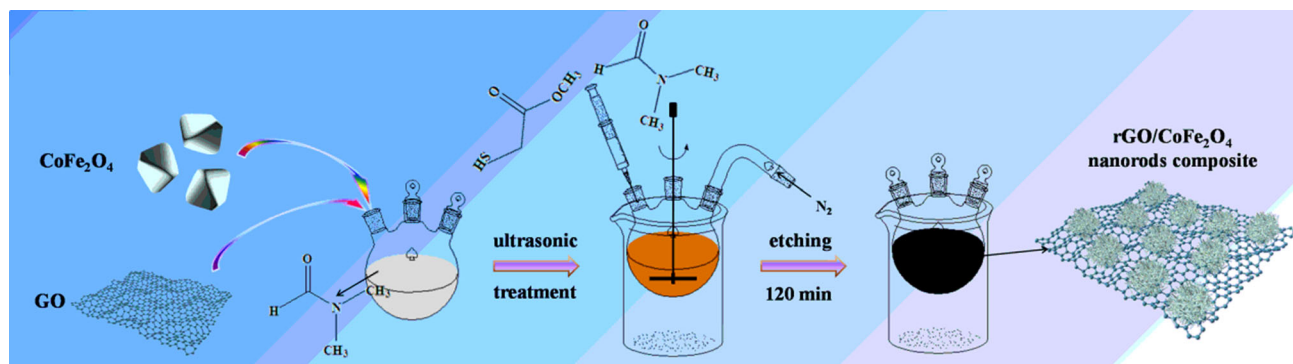
Scheme 1 The schematic illustration of the preparation of the rGO/Co$_2$FeO$_4$ nanorods composite

precipitate and NaCl were mixed according to the mass ratio of 1:1 and calcined at 1000 °C for 4 h. The mixture of CoFe$_2$O$_4$ and NaCl was washed with ultrapure water to remove the NaCl. At last, the CoFe$_2$O$_4$ particles were obtained.

2.3 Preparation of rGO/CoFe$_2$O$_4$ nanorods composite

0.2 g above CoFe$_2$O$_4$ particles and a proper amount (50, 60, 70, 80 mg) of prepared GO were sufficient dissolved in DMF in a three-necked bottle at 80 °C. Subsequently, 10 mL of NH$_2$NH$_2$·H$_2$O and 2.5 mL of C$_3$H$_6$O$_2$S were added to the above solution under N$_2$ atmosphere dropwisely with continuously stirring. After 2 h, the reaction was terminated with cold ethanol. Finally, the precipitate was pulpified alternately with ethanol and ultrapure water, followed by freeze-dried for 24 h. According to the different amounts of GO nanosheets (50, 60, 70, 80 mg), the obtained rGO/CoFe$_2$O$_4$ nanorods composites were named S-50, S-60,S-70 and S-80, separately. The preparation of the rGO/CoFe$_2$O$_4$ nanorods composites is investigated in Scheme 1.

2.4 Materials characterization

The morphologies and structures of rGO/CoFe$_2$O$_4$ nanorods composite were recorded by scanning electron microscopy (SEM, Hitachi, S-4800, Japan) equipped with energy dispersive X-ray analysis (EDX), and transmission electron microscopy (TEM, JEOL-2010, Japan). The specific surface area and pore size distribution were determined by the Brunner–Emmet–Teller method (BET, ASAP 2020, Micromeritics). The crystal structures of obtained products were observed by X-ray diffraction (XRD,

D/max-2200, Japan). The carbon graphitization degree was investigated by Raman spectra (Raman, Horiba JobinYvon, France).

The EM parameters (ε', ε'', μ, μ'') of samples were characterized by vector network analyzer (VNA, HP8720ES, Agilent, USA) through the coaxial wire method in the frequency range of 2–18 GHz. rGO/CoFe$_2$O$_4$ nanorods composites (30 wt%) were mixed with molten wax (70 wt%) and compacted into coaxial rings (d_{in}=3.04 mm, d_{out}=7 mm, and t = 3 mm).

3 Results and discussion

3.1 Structure and morphology of rGO/CoFe$_2$O$_4$ nanorods composite

Figure 1a illustrates the XRD patterns of the rGO, CoFe$_2$O$_4$ particles, CoFe$_2$O$_4$ nanorods and rGO/CoFe$_2$O$_4$ nanorods composite. Apparently, it appears a broad diffraction peak at about $2\theta = 25°$ that correlates to the graphite-like structure (002) with an interlayer spacing of 0.36 nm in the XRD pattern of rGO, indicating that the GO has been changed to rGO [29]. The diffraction peaks for CoFe$_2$O$_4$ particles and CoFe$_2$O$_4$ nanorods are well matched with CoFe$_2$O$_4$ cubic spinel crystal structure (JCPDS card no. 22-1086). Remarkably, the intensity for the CoFe$_2$O$_4$ nanorods presents a significant drop compared with CoFe$_2$O$_4$ particles because the porous structure contains abundant tiny fragments. For rGO/CoFe$_2$O$_4$ nanorods composite, all the observed peaks correspond to CoFe$_2$O$_4$ and there are no other peaks, demonstrating the purity of rGO/CoFe$_2$O$_4$ nanorods composite. The diffraction pattern of rGO is not observed in rGO/CoFe$_2$O$_4$ nanorods composites
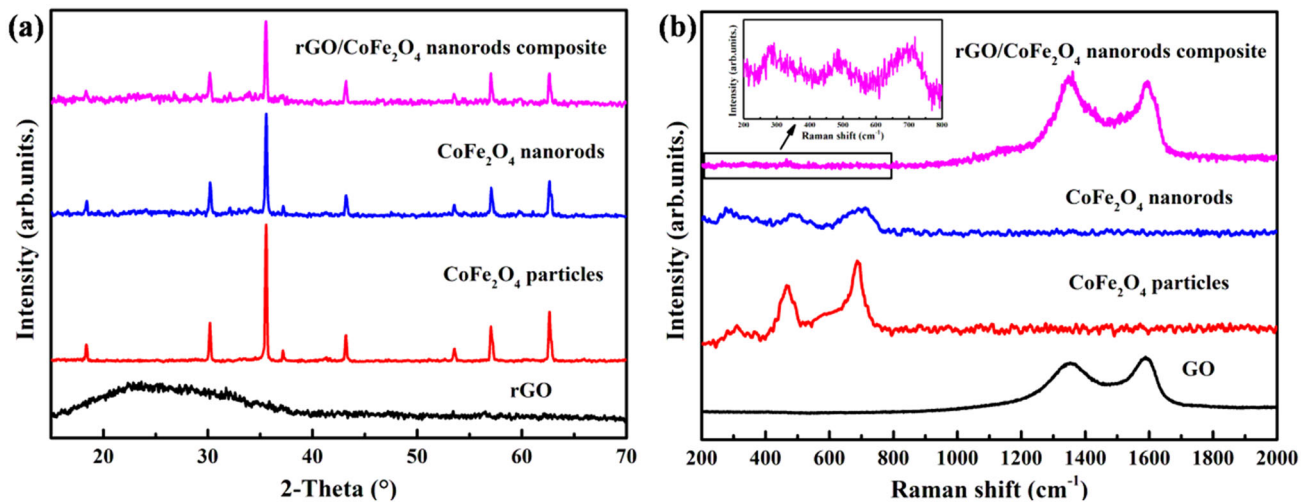
Fig. 1 **a** XRD spectra and **b** Raman spectra of the as-prepared samples

because the diffraction intensity of rGO may be too weak compared with that of the $CoFe_2O_4$ crystals.

The Raman spectra are investigated to reveal the structural information of composites (Fig. 1b). The Raman spectrum of GO has two prominent peaks at 1352 cm^{-1} (D band) and 1589 cm^{-1} (G band). The former represents the defect and disorder of carbon materials and the latter stands for the in-plane vibration modes of carbon atoms [30]. Three clear and prominent peaks located at about 311, 468 and 690 cm^{-1} in the spectrum of $CoFe_2O_4$ particles are detected, which is consistent with the characteristic bands of $CoFe_2O_4$ [31, 32]. The peak positions of $CoFe_2O_4$ nanorods are still in accordance with that of $CoFe_2O_4$ particles, but the intensities decrease, which corresponds to the XRD results. Further, the intensity ratio (I_D/I_G) is used to estimate the defect densities [33]. The intensity ratio of rGO/$CoFe_2O_4$ nanorods composite (S-70) ($I_D/I_G = 1.02$) is bigger than that of GO ($I_D/I_G = 0.91$), indicating that many defects and disorders exist in S-70 [15, 20]. Meanwhile, the disorder nature is important for superior EM absorption materials [22].

The SEM and TEM images of $CoFe_2O_4$ particles, $CoFe_2O_4$ nanorods and rGO/$CoFe_2O_4$ nanorods composite (S-70) are displayed in Fig. 2. As shown in Fig. 2a, d, $CoFe_2O_4$ particles have a typical spinel morphology with a size of ~ 500 nm. And the nanorod-like $CoFe_2O_4$ powders with a length of about 300 nm were observed after etching process (Fig. 2b, e). As can be seen from Fig. 2c, $CoFe_2O_4$ nanorods are densely embedded in the flexible rGO

sheets, meaning good adhesion between rGO and $CoFe_2O_4$ nanorods. The force between the rGO and $CoFe_2O_4$ is molecular force. The evolution of nanorods of $CoFe_2O_4$ may be attributed to the loss of $CoFe_2O_4$ which due to the reduction of Fe^{3+} to Fe^{2+} by hydrazine. Then, Fe^{2+} is immediately coordinated with methyl mercaptoacetate in DMF, which results in the removing of $CoFe_2O_4$. Thus, $CoFe_2O_4$ nanorods are formed on surfaces of rGO. TEM images of rGO/$CoFe_2O_4$ nanorods composite (S-70) further reveal $CoFe_2O_4$ nanorods wrapped by rGO sheets.

The nitrogen absorption–deposition isotherm analysis of the $CoFe_2O_4$ particles, $CoFe_2O_4$ nanorods and rGO/$CoFe_2O_4$ nanorods composite (S-70) was investigated to study the surface area. As presented in Fig. 3, the samples showed typical IV isotherms, demonstrating their mesoporous character [34]. The surface areas are 0.94, 9.05 and $15.10 \text{ m}^2 \text{ g}^{-1}$ for $CoFe_2O_4$ particles, $CoFe_2O_4$ nanorods and rGO/$CoFe_2O_4$ nanorods composite (S-70), respectively. The larger the surface area, the more active sites for the effective reflecting and scattering EM waves can be provided, which may be good for the multiple absorption processes of EM waves.

The phase compositions of the as-synthesized rGO/$CoFe_2O_4$ nanorods composite with different rGO contents are measured by XRD (Fig. 4). All the diffraction peaks are well assigned to the standard card of the spinel structured $CoFe_2O_4$. And the peak at around 25° belonging to (002) crystal face of rGO cannot be indexed in composites, confirming that the intensity of rGO/$CoFe_2O_4$ nanorods composite peaks
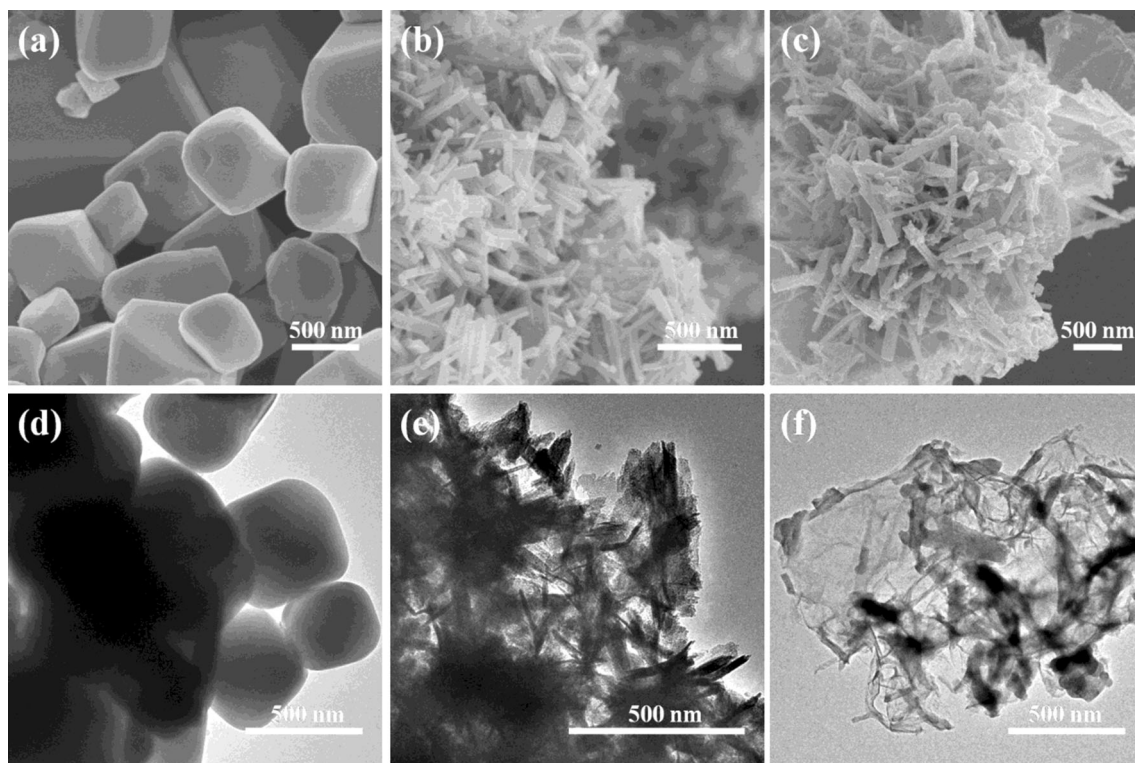
Fig. 2 SEM images of **a** CoFe$_2$O$_4$ particles, **b** CoFe$_2$O$_4$ nanorods and **c** rGO/CoFe$_2$O$_4$ nanorods composite (S-70); TEM images of **d** CoFe$_2$O$_4$ particles, **e** CoFe$_2$O$_4$ nanorods and **f** rGO/CoFe$_2$O$_4$ nanorods composite (S-70)
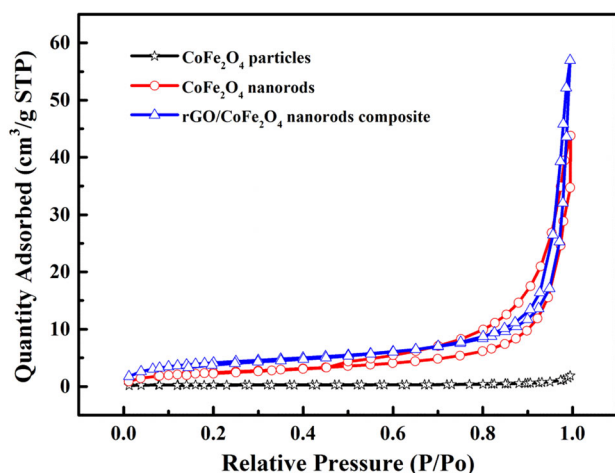
Fig. 3 N$_2$ adsorption–desorption isotherms of the prepared CoFe$_2$O$_4$ particles, CoFe$_2$O$_4$ nanorods and rGO/CoFe$_2$O$_4$ nanorods composite (S-70)

Fig. 4 XRD patterns of rGO/CoFe$_2$O$_4$ nanorods composite with different rGO contents

is very strong. Meanwhile, no other unclear peaks appear, suggesting the purity of rGO/CoFe$_2$O$_4$ nanorods composite.

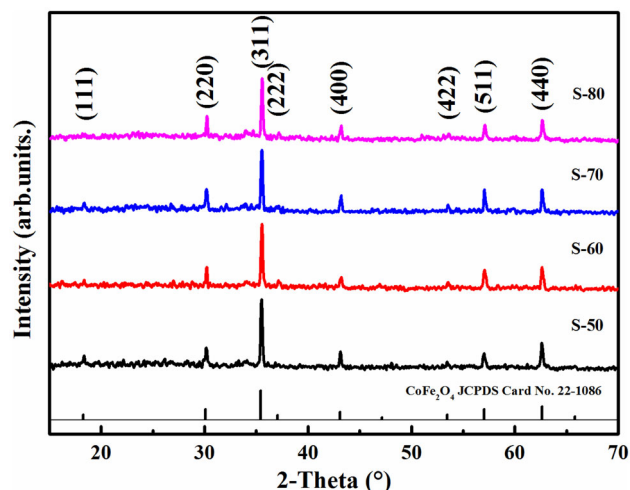Typical morphology of the as-synthesized rGO/CoFe$_2$O$_4$ nanorods composite (S-70) is shown in Fig. 5a–d. The composite is consisted with flexible 2D sheet-like rGO and 3D nanorods. The larger magnification SEM images of rGO/CoFe$_2$O$_4$ nanorods composite (S-70) clearly show that the composite is assembled by numerous CoFe$_2$O$_4$ nanorods grown on rGO nanosheets, generating multiple interfaces in 3D hierarchical microstructures. Further, the composition of the rGO/CoFe$_2$O$_4$ nanorods composite further

analyzed by elemental mapping through EDS (Fig. 5e). The distributions of C, O, Fe and Co elements with different colors, implying the interconnection of CoFe$_2$O$_4$ nanorods and rGO.

3.2 EM wave absorption properties of rGO/ CoFe$_2$O$_4$ nanorods composite

The RL values for the rGO/CoFe$_2$O$_4$ nanorods composite were obtained by using the transmission line theory. They are calculated by experimentally obtaining electromagnetic parameters. The equations are as below [35–38]:

$$Z_{in} = Z_0 \sqrt{\frac{\mu_r}{\varepsilon_r}} \tan h \left[j \frac{2\pi}{c} \sqrt{\mu_r \varepsilon_r} f d \right] \quad (1)$$

$$RL(dB) = 20 lg \left| \frac{Z_{in} - Z_0}{Z_{in} + Z_0} \right|, \quad (2)$$

where Z_{in} represents the input impedance of the absorber, Z_0 means the characteristic impedance of free space, ε_r and μ_r are complex permittivity and permeability of the absorber, respectively. f is the frequency, d is the thickness of the specimen, and c is the velocity of light. Figure 6 is the RL–f curves of composites with different thicknesses. The amount of rGO introduced has significant influences on the EM wave absorbing capacities of samples. From Fig. 6a

Fig. 6 Frequency dependence of reflection loss (**a–d**) and the ▶ corresponding 3D contour maps of reflection loss versus frequency and thickness (**e–h**) for rGO/CoFe$_2$O$_4$ nanorods composite with different mass ratios of rGO

and e, the RL of S-50 is relatively poor with only − 6.9 dB at 2.4 mm. Further increasing the rGO content to 60 mg (S-60), the RL$_{max}$ is − 16.2 dB at 14.4 GHz with 2 mm and the corresponding EAB is 3.1 GHz (from 12.5 to 15.6 GHz) (Fig. 6b and f). As shown in Fig. 6c and g, the composite of S-70 exhibits the best absorption performance than other composites. The RL$_{max}$ reaches − 56.3 dB and the EAB is 3.4 GHz (14.6–18 GHz) at 1.4 mm. In addition, the EAB range can be well adjusted by changing the thickness. When the thickness is increased to 1.6 mm, the EAB is 4.3 GHz and the RL$_{max}$ value is − 26.4 dB. According, the excellent microwave absorption properties of S-70 may be ascribed to impedance matching characteristic and/or EM wave attenuation. Figure S1 shows the RL curves of CoFe$_2$O$_4$ particles and CoFe$_2$O$_4$ nanorods with various thicknesses. The RL$_{max}$ value of CoFe$_2$O$_4$ particles and CoFe$_2$O$_4$ nanorods is − 14.1 dB and − 33.1 dB at 3 mm. Compared with CoFe$_2$O$_4$ particles, the RL$_{max}$ value of CoFe$_2$O$_4$ nanorods is significantly increased, which may be due to its larger specific surface area. CoFe$_2$O$_4$
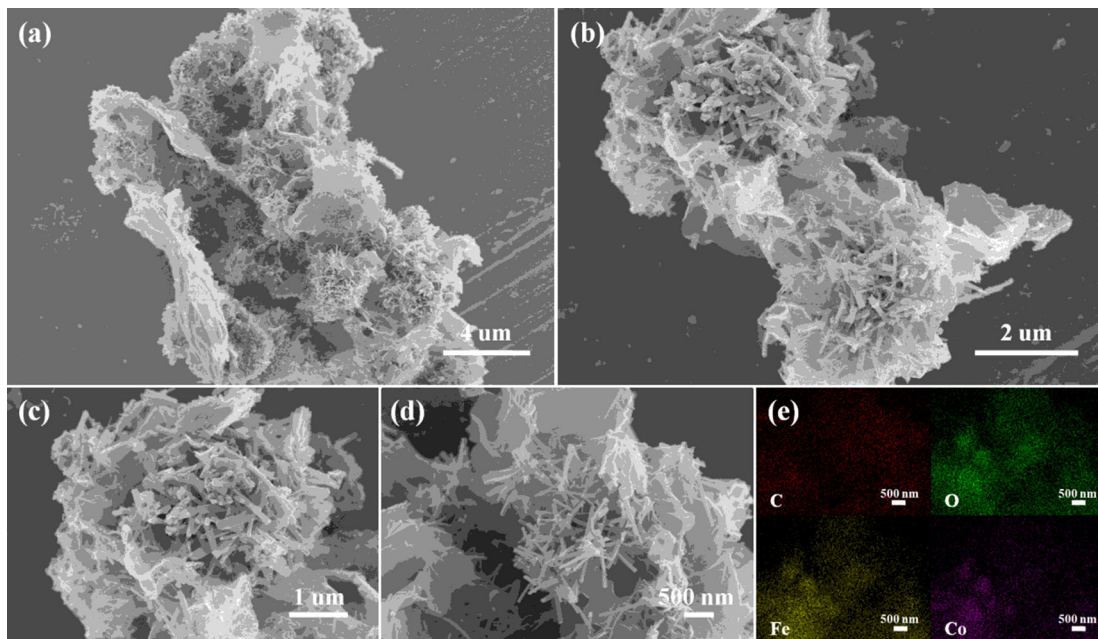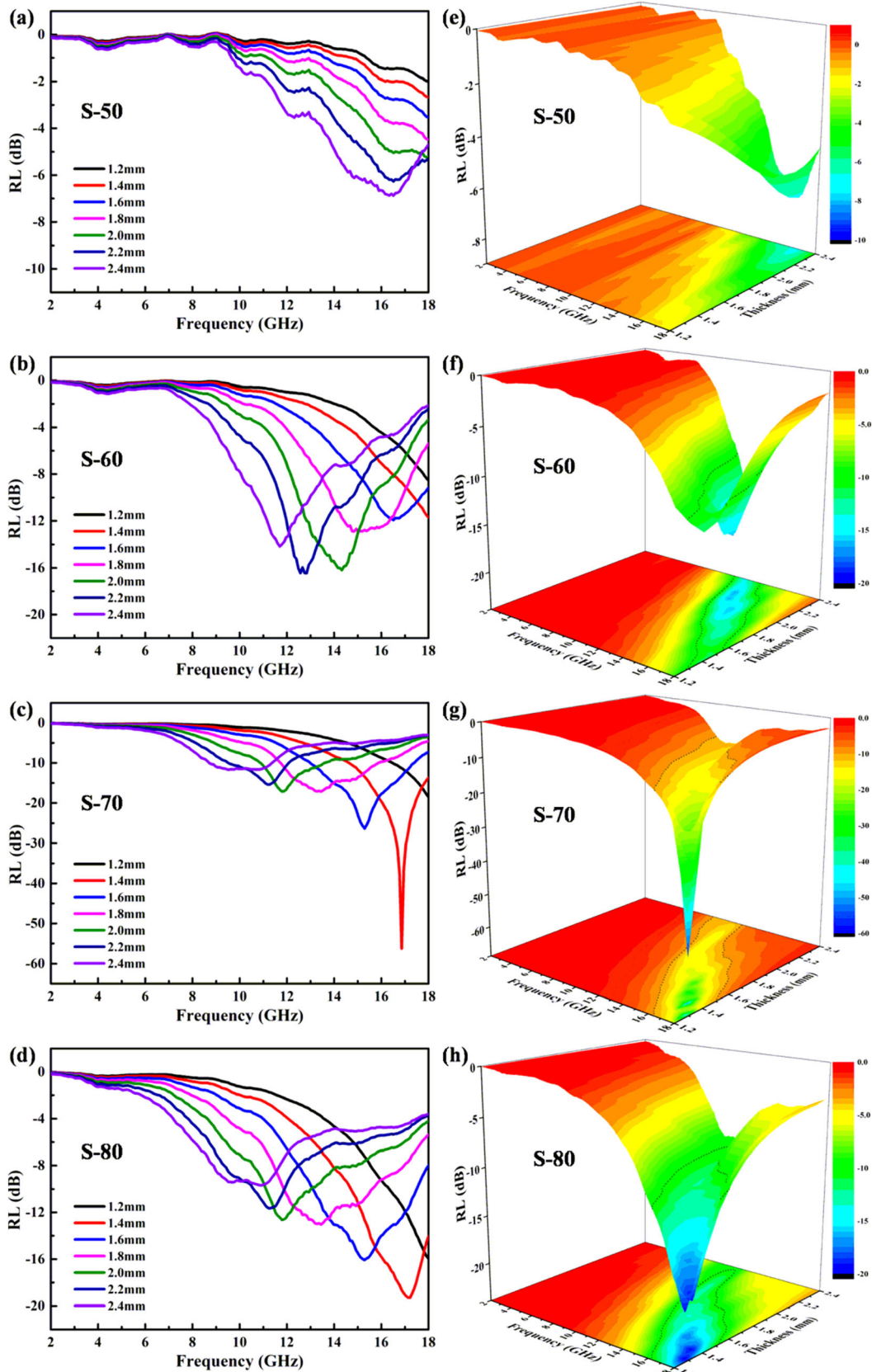

Fig. 5 SEM images with different magnifications (**a–d**), elemental mapping (**e**) of C, O, Fe and Co of rGO/CoFe$_2$O$_4$ nanorods composite (S-70)

nanorods possess high surface area, which provide more active sites for the effective reflection and scattering of incident electromagnetic. Nevertheless, the RL_{max} values of both are lower than those of S-70. For S-80 in Fig. 6d and h, compared with S-70, the maximum RL value and the effective absorption frequency width are significantly reduced. Consequently, only when the amount of rGO is suitable can the absorbing property of the absorber be improved.

The microwave absorption properties of the absorbers usually are dependent on relative complex permittivity ($\varepsilon_r = \varepsilon' - j\varepsilon''$) and relative complex permeability ($\mu_r = \mu' - j\mu''$). The real part and the imaginary part represent the storage capability and loss ability [39–41]. The dielectric loss tangent (tan $\delta_\varepsilon = \varepsilon''/\varepsilon'$) and the magnetic loss tangent (tan $\delta_\mu = \mu''/\mu'$) indicate the dielectric loss and magnetic loss [42], respectively.

The function of ε', ε'', μ', μ'', tan δ_ε and tan δ_μ with frequency over 2–18 GHz for the rGO/CoFe$_2$O$_4$ nanorods composites (S-50, S-60, S-70 and S-80) is shown in Fig. 7, respectively. The ε' and ε'' values of rGO/CoFe$_2$O$_4$ nanorods composite are proportional to the introduction of rGO sheets, but inversely proportional to the frequency, which is a normal for dielectrics (Fig. 7a and b) [43–47]. The ε' values for S-50, S-60, S-70 and S-80 range from 3.8 to 6.6, 5.8–14.3, 8.2–25.7, and 8.7–30.5 in 2–18 GHz, respectively. And the curve of ε'' has a similar trend to the curve of ε'. The ε' and ε'' of the CoFe$_2$O$_4$ particles and CoFe$_2$O$_4$ nanorods are shown in Fig. S2 (a and b), which are much lower than those of the rGO/CoFe$_2$O$_4$ nanorods composite. This phenomenon reveals that introducing rGO nanosheets can greatly improve the permittivity of rGO/CoFe$_2$O$_4$ nanorods composite due to the high electrical conductivity property of rGO. Besides, the residual defects and groups of rGO surface bring the relaxation and polarization that increase the permittivity over 2–18 GHz. Figure 7c and d presents relationship between complex permeability (μ' and μ'') and frequency for rGO/CoFe$_2$O$_4$ nanorods composites. The μ' and μ'' values of rGO/CoFe$_2$O$_4$ nanorods composites do not differ significantly with different rGO proportions. This is because the introduced rGO is a non-magnetic material that will not influence the magnetic properties of the rGO/CoFe$_2$O$_4$ nanorods composite. The μ' and μ'' of the CoFe$_2$O$_4$ particles and CoFe$_2$O$_4$ nanorods are illustrated in Fig. S2 (c and d). They do not change a lot with increasing the frequency. The curves of tan δ_ε and tan δ_μ show obviously

fluctuation over 2–18 GHz (Fig. 7e and f). And as rGO nanosheets are increased, tan δ_ε is strengthened. Here, as to S-70, the dielectric loss is much higher than magnetic loss in the frequency range of 2–15 GHz, which denotes that the EM loss in the lower frequency mainly comes from dielectric loss but the magnetic loss mainly contributes in the higher frequency. The results display that the adjustment of rGO amount has great tunable potential for EM impedance matching.

Generally speaking, the microwave absorption ability mainly relies on the impedance matching ($|Z_{in}/Z_0|$) and attenuation constant (α). The impedance matching characteristic is a prerequisite for achieving excellent microwave absorber [48]. When value of $|Z_{in}/Z_0|$ approaches to one, most of the EM waves can enter the absorber. Then they are effectively transformed to other forms of energy, or dissipated at the air–absorber interface. Nevertheless, the α is another important factor to determine the absorbing properties of absorbing materials. High α can effectively attenuate or transform the incident microwave. The α can be expressed as the following equation [49]:

$$\alpha = \frac{\sqrt{2}\pi f}{c}$$
$$\times \sqrt{(\mu''\varepsilon'' - \mu'\varepsilon') + \sqrt{(\mu''\varepsilon'' - \mu'\varepsilon')^2 + (\mu'\varepsilon'' + \mu''\varepsilon')^2}}. \tag{3}$$

Figure 8 presents the EM $|Z_{in}/Z_0|$ and α of rGO/CoFe$_2$O$_4$ nanorods composite with different rGO proportions. The $|Z_{in}/Z_0|$ values of S-70 are closer to 1 among four composites in the whole frequency range at 1.4 mm (Fig. 8a), indicating that S-70 has the best impedance matching. From Fig. 8b, S-70 and S-80 show much higher α than other composites. However, the EM absorption performance of S-80 is not as good as that of S-70, illustrating that the superior microwave absorber not only influenced by comprehensive attenuation ability, but also by impedance matching characteristics.

The magnetic loss of rGO/CoFe$_2$O$_4$ nanorods composite mainly comes from the CoFe$_2$O$_4$ nanorods. Normally, the magnetic loss is basically originated from hysteresis loss, domain wall resonance, eddy current loss, natural resonance and exchange resonance [50–52]. Hysteresis loss and domain wall resonance loss always occur at low frequency (MHz). The eddy current loss donation contribution is decided from $C_0 = \mu''(\mu')^{-2}f^{-1}$ [53]. When the magnetic
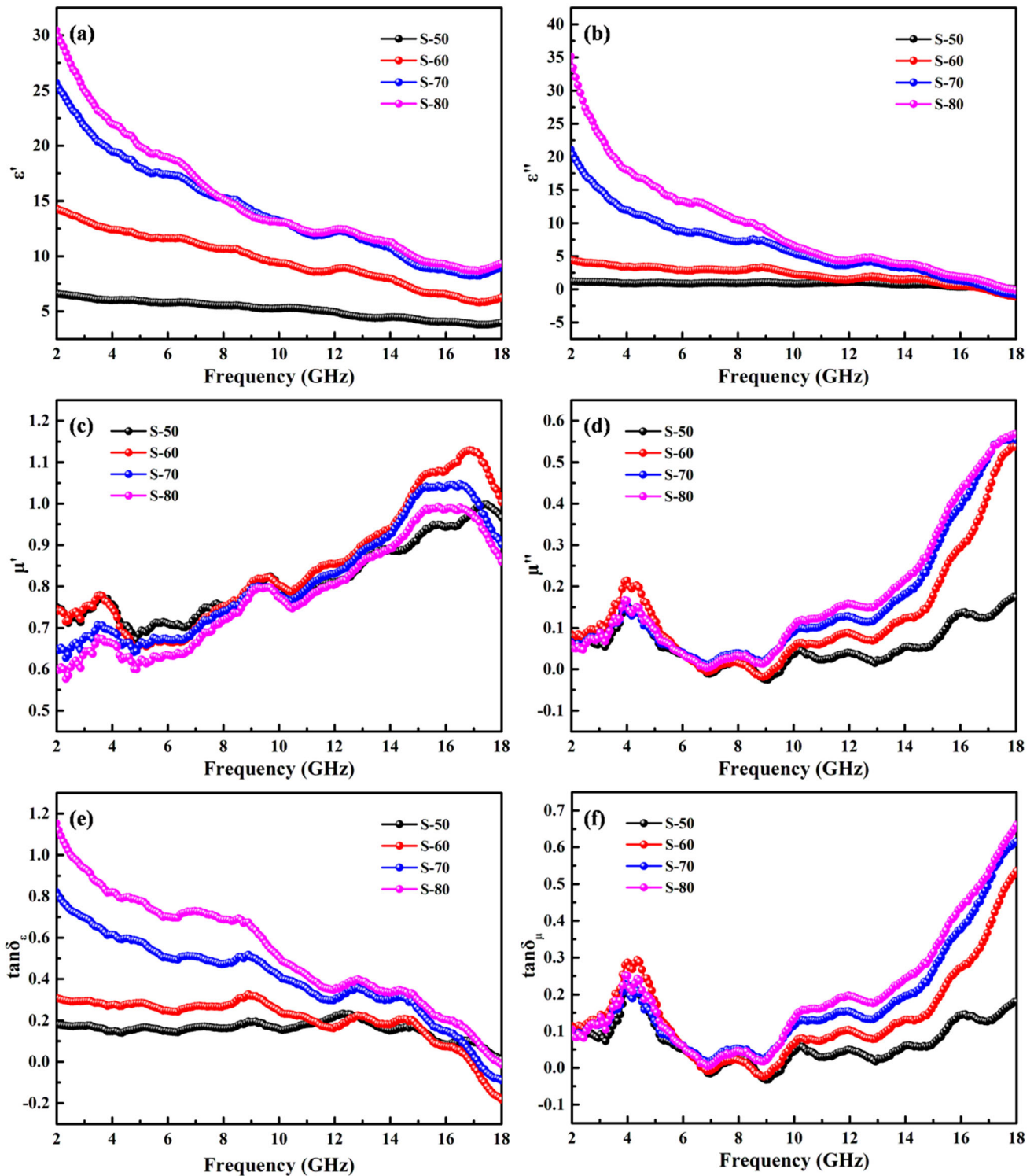
Fig. 7 Frequency dependence of the real part (**a**) and imaginary part (**b**) of relative complex permittivity, real part (**c**) and imaginary part (**d**) of relative complex permeability, dielectric loss (**e**) and magnetic loss (**f**) for rGO/CoFe$_2$O$_4$ nanorods composite with different mass ratios of rGO
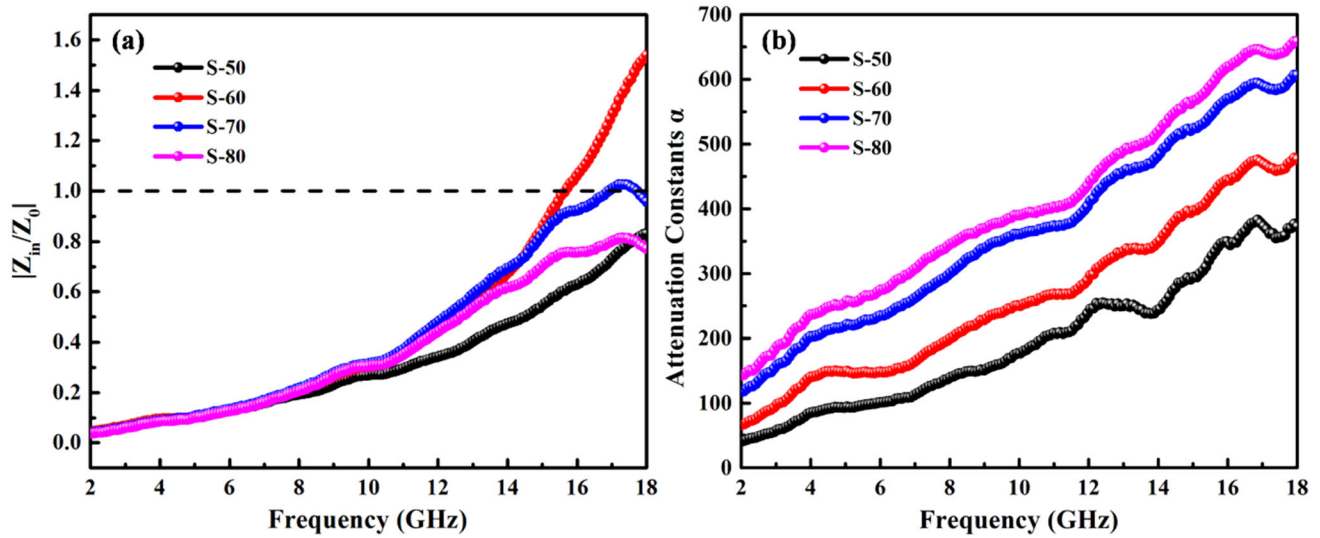
Fig. 8 The impedance matching (**a**) and attenuation constants α (**b**) versus frequency for all samples

loss originates from the eddy current loss, the value of C_0 remains unchanged [54]. Figure 9 illustrates the C_0-f curves of four samples. A noticeable variation can be detected, suggesting the inexistence of eddy current effect. From the above results, the natural resonance and exchange resonance are the main forms of magnetic loss of rGO/CoFe$_2$O$_4$ nanorods composite. Meanwhile, the significant variation of C_0 at 2–7 GHz is basically because of the natural resonance, while at higher frequency the exchange resonance loss dominates.

Scheme 2 shows the proposed EM wave absorbing mechanism of the rGO/CoFe$_2$O$_4$ nanorods absorber. The absorbing property comprehensively depends on the impedance matching, dielectric loss and magnetic loss mechanisms [55]. Firstly, combining CoFe$_2$O$_4$ nanorods with rGO provides dielectric loss and magnetic loss. The optimal impedance matching is a prerequisite to allow EM waves to get into the absorbers to the maximum extent [56]. Secondly, the interfaces among rGO/rGO, rGO/air and rGO/CoFe$_2$O$_4$ nanorods induce lots of interfacial polarization. The interface polarization caused by multiple interfaces converts EM wave energy into thermal energy [55]. Thirdly, the defects and function groups in rGO provide many dipoles resulting in polarization and relaxation loss [50, 57]. Finally, the special structure of rGO/CoFe$_2$O$_4$ nanorods composite is prone to multiple reflections, which is beneficial to improve the EM wave absorbing performance [58–60].
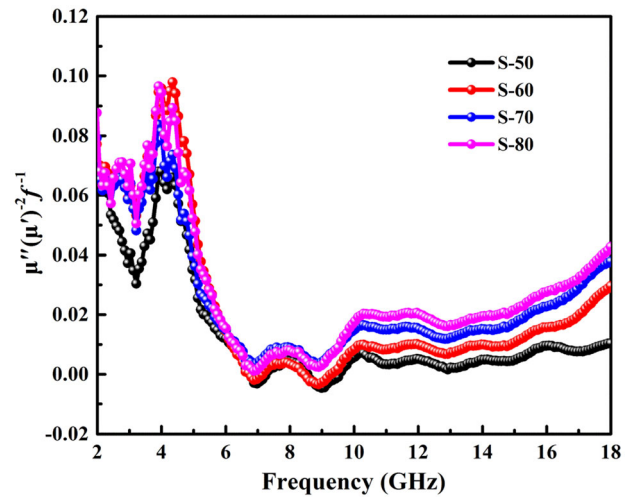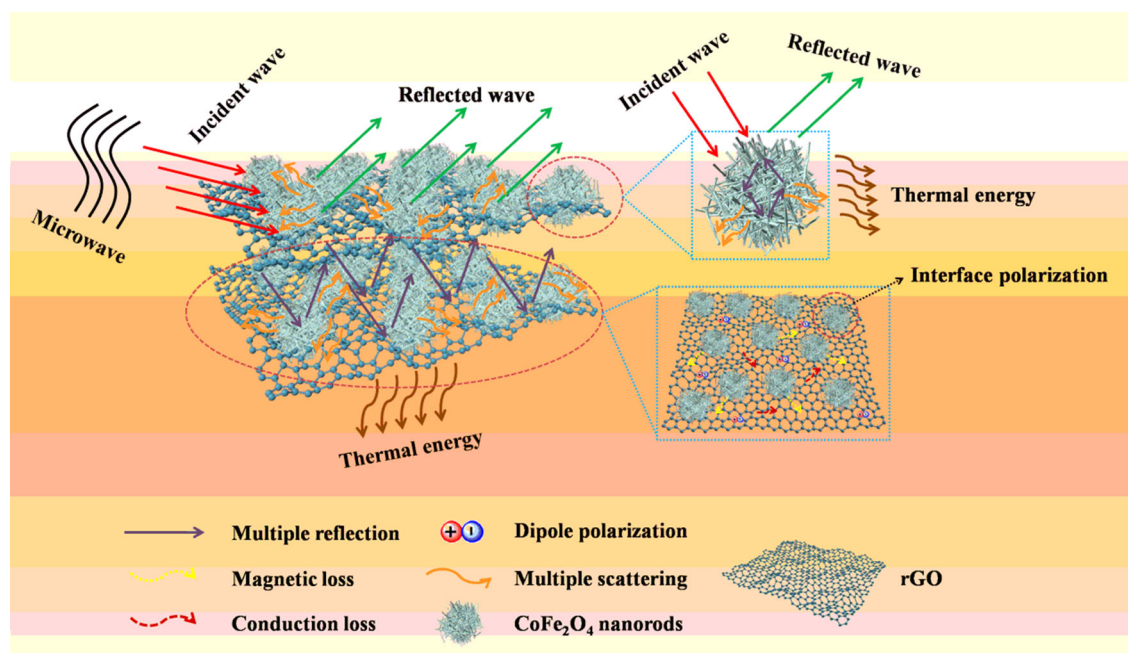

Fig. 9 $\mu''(\mu')^{-2}f^{-1}$ values of rGO/CoFe$_2$O$_4$ nanorods composite with different mass ratios of rGO

EM wave absorbing performances of rGO/CoFe$_2$O$_4$ nanorods composite and other metal oxide composites are displayed in Table 1. Compared with most of them [61–69], rGO/CoFe$_2$O$_4$ nanorods composite (S-70) revealed outstanding performance at a thin thickness, which meet the requirement of "thin, strong, light, wide". Thus, rGO/CoFe$_2$O$_4$ nanorods composite can be theoretically used as a high-efficient and controllable microwave absorbers.

Scheme 2 Possible mechanism for the microwave absorption of rGO/CoFe$_2$O$_4$ nanorods composite

Table 1 EM wave absorbing performances of rGO/CoFe$_2$O$_4$ nanorods composite and other metal oxide composites

Material	Matrix	Absorber content	Optimum frequency (GHz)	Optimum thickness (mm)	R_L (dB)	Bandwidth (GHz)	References
rGO/Fe$_3$O$_4$	Paraffin	50 wt%	12.07	2.5	− 18.2	2	[61]
rGO/ZnO	Paraffin	50 wt%	9.7	2.2	− 45.05	2.5	[62]
rGO/β-LiFe$_5$O$_8$	Paraffin	40 wt%	16.5	9	− 26.3	2.5	[63]
rGO/ZnFe$_2$O$_4$	Paraffin	30 wt%	16.7	1.6	− 29.3	2.6	[64]
rGO/BiFeO$_3$	PVA	10 wt%	10.68	1.55	− 28.68	2.1	[65]
rGO/Ni$_{0.8}$Zn$_{0.2}$Fe$_2$O$_4$	Paraffin	50 wt%	10.6	2.0	− 18.4	3.32	[66]
PEDOT/rGO/Co$_3$O$_4$	Paraffin	50 wt%	10.7	2.0	− 51.1	3.1	[67]
MoS$_2$/Fe$_3$O$_4$/graphene	Paraffin	30 wt%	5.9	2.5	− 45.8	5.1	[68]
rGO-Fe$_3$O$_4$@ZnO	Epoxy	30 wt%	11.4	5	− 38.0	2.4	[69]
rGO/CoFe$_2$O$_4$ nanorods composite	Paraffin	30 wt%	16.9	1.4	− 56.3	3.4	This work

4 Conclusions

CoFe$_2$O$_4$ nanorods anchored on rGO nanosheets have been successfully prepared via etching method. The as-prepared rGO/CoFe$_2$O$_4$ nanorods composite presents superior microwave absorption properties. Different amounts of GO nanosheets are introduced in the composite to support the CoFe$_2$O$_4$ nanorods. The results suggest that the optimal RL value of rGO/CoFe$_2$O$_4$ nanorods composite (S-70) could reach − 56.3 dB with a thickness of 1.4 mm along with an EAB of 3.4 GHz. And the heterostructure of rGO/CoFe$_2$O$_4$ nanorods composite could be widely applied as strong capacity and lightweight microwave absorbing materials.

Acknowledgements

References

1. W. Xu, G.S. Wang, P.G. Yin, Designed fabrication of reduced graphene oxides/Ni hybrids for effective electromagnetic absorption and shielding. Carbon **139**, 759–767 (2018)

2. X.J. Zhang, G.S. Wang, W.Q. Cao, Y.Z. Wei, J.F. Liang, L. Guo, M.S. Cao, Enhanced microwave absorption property of reduced graphene oxide (RGO)-$MnFe_2O_4$ nanocomposites and polyvinylidene fluoride. ACS Appl. Mater. Interface **6**, 7471–7478 (2014)

3. X.H. Liang, Z.M. Man, B. Quan, J. Zheng, W.H. Gu, Z. Zhang, G.B. Ji, Environment-stable Co_xNi_y encapsulation in stacked porous carbon nanosheets for enhanced microwave absorption. Nano-Micro Lett. **12**, 102 (2020)

4. H.L. Lv, G.B. Ji, W. Liu, H.Q. Zhang, Y.W. Du, Achieving hierarchical hollow carbon@Fe@Fe_3O_4 nanospheres with superior microwave absorption properties and lightweight features. J. Mater. Chem. C **3**, 10232–10241 (2015)

5. Y. Cheng, J.Z.Y. Seow, H.Q. Zhao, Z.C.J. Xu, G.B. Ji, A flexible and lightweight biomass–reinforced microwave absorber. Nano-Micro Lett. **12**, 125 (2020)

6. W.H. Gu, J.W. Tan, J.B. Chen, Z. Zhang, Y. Zhao, J.W. Yu, G.B. Ji, Multifunctional bulk hybrid foam for infrared stealth, thermal Insulation, and microwave absorption. ACS Appl. Mater. Interface **12**, 28727–28737 (2020)

7. H.B. Yang, B. Wen, L. Wang, Carbon nanotubes modified CoZn/C composites with rambutan-like applied to electromagnetic wave absorption. Appl. Surf. Sci. **509**, 145336 (2020)

8. Y. Wang, X. Gao, X.M. Wu, C.Y. Luo, Facile synthesis of Mn_3O_4 hollow polyhedron wrapped by multiwalled carbon nanotubes as a high-efficiency microwave absorber. Ceram. Int. **46**, 1560–1568 (2020)

9. X.H. Liang, B. Quan, Z.M. Man, B.C. Cao, N. Li, C.H. Wang, G.N. Ji, T. Yu, Self-assembly three-dimensional porous carbon networks for efficient dielectric attenuation. ACS Appl. Mater. Interface **11**, 30228–30233 (2019)

10. H. Wang, Y. Zheng, W. Cui, Y. Sun, D. Zhang, Interface polarization strategy to prepare Sn/SnO_2@C absorber with tunable core compositions and broader frequency absorption properties. Appl. Surf. Sci. **455**, 1057–1062 (2018)

11. Z. Zhang, X. Chen, Z. Wang, L. Heng, S. Wang, Z. Tang, Y. Zou, Carbonyl iron/graphite microspheres with good impedance matching for ultra-broadband and highly efficient electromagnetic absorption. Opt. Mater. Express **11**, 3319–3331 (2018)

12. S. Wang, S. Peng, S. Zhong, W. Jiang, Construction of SnO_2/Co_3Sn_2@C and SnO_2/Co_3Sn_2@Air@C hierarchical heterostructures for efficient electromagnetic wave absorption. J. Mater. Chem. C **6**, 9465–9474 (2018)

13. H. Zhao, Y. Cheng, W. Liu, Z. Yang, B. Zhang, G. Ji, Y. Du, The flaky porous Fe_3O_4 with tunable dimensions for enhanced microwave absorption performance in X andC bands. Nanotechnology **29**, 295603 (2018)

14. J. Yan, Y. Huang, C. Chen, X.D. Liu, H. Liu, The 3D CoNi alloy particles embedded in N-doped porous carbon foams for high-performance microwave absorbers. Carbon **152**, 545–555 (2019)

15. H. Zhang, A.J. Xie, C.P. Wang, H.S. Wang, Y.H. Shen, X.Y. Tian, Novel rGO/α-Fe_2O_3 composite hydrogel: synthesis, characterization and high performance of electromagnetic wave absorption. J. Mater. Chem. A **1**, 8547–8552 (2013)

16. K.S. Novoselov, A.K. Geim, S.V. Morozov, D. Jiang, Y. Zhang, S.V. Dubonos, I.V. Grigorieval, A.A. Firsov, Electric field effect in atomically thin carbon films. Science **306**, 666–669 (2014)

17. N. Yousefi, X.Y. Sun, X.Y. Lin, X. Shen, J.J. Jia, B. Zhang, B.Z. Tang, M.S. Chan, J.K. Kim, Highly aligned graphene/polymer nanocomposites with excellent dielectric properties for high-performance electromagnetic interference shielding. Adv. Mater. **26**, 5480–5487 (2014)

18. Y.F. Pan, G.S. Wang, L. Liu, L. Guo, S.H. Yu, Binary synergistic enhancement of dielectric and microwave absorption properties: a composite of arm symmetrical PbS dendrites and polyvinylidene fluoride. Nano Res. **10**, 284–294 (2017)

19. Z. Li, X. Li, Y. Zong, G. Tan, Y. Sun, Y. Lan, M. He, Z. Ren, X. Zheng, Solvothermal synthesis of nitrogen-doped grapheme decorated by superparamagnetic Fe_3O_4 nanoparticles and their applications as enhanced synergistic microwave absorbers. Carbon **115**, 493–502 (2017)

20. D. Chen, G.S. Wang, S. He, J. Liu, L. Guo, M.S. Cao, Controllable fabrication of mono-dispersed RGO-hematite nanocomposites and their enhanced wave absorption properties. J. Mater. Chem. A **1**, 5996–6003 (2013)

21. K.Y. Chen, C. Xiang, L.C. Li, H.S. Qian, Q.S. Xiao, F. Xu, A novel ternary composite: fabrication, performance and application of expanded graphite/polyaniline/CoFe₂O₄ ferrite. J. Mater. Chem. **22**, 6449–6455 (2012)

22. N. Zhang, Y. Huang, P. Liu, X. Ding, M. Zong, M. Wang, Synthesis of magnetical nanoparticles decorated with reduced graphene oxide as an efficient broad band EM wave absorber. J. Alloy Compd. **692**, 639–646 (2017)

23. S.L. Zhang, Q.Z. Jiao, Y. Zhao, H.S. Li, Q. Wu, Preparation of rugby-shaped CoFe₂O₄ particles and their microwave absorbing properties. J. Mater. Chem. A **2**, 18033–18039 (2014)

24. X.H. Li, J. Feng, Y.P. Du, J.T. Bai, H.M. Fan, H.L. Zhang, Y. Peng, F.S. Li, One-pot synthesis of CoFe₂O₄/graphene oxide hybrids and their conversion into FeCo/graphene hybrids for lightweight and highly efficient microwave absorber. J. Mater. Chem. A **3**, 5535–5546 (2015)

25. B. Zhang, J. Wang, J.P. Wang, H.J. Duan, S.Q. Huo, Y.S. Tang, Coprecipitation synthesis of hollow poly(acrylonitrile) microspheres@CoFe₂O₄ with graphene as lightweight microwave absorber. J. Mater. Sci.: Mater. Electron. **28**, 3337–3348 (2017)

26. D. Moitra, M. Chandel, B.K. Ghosh, R.K. Jani, M.K. Patra, S.R. Vaderab, N.N. Ghosh, A simple 'in situ' co-precipitation method for the preparation of multifunctional CoFe₂O₄–reduced graphene oxide nanocomposites: excellent microwave absorber and highly efficient magnetically separable recyclable photocatalyst for dye degradation. RSC Adv. **6**, 76759–76772 (2016)

27. M. Fu, Q. Jiao, Y. Zhao, H. Li, Vapor diffusion synthesis of CoFe₂O₄ hollow sphere/graphene composites as absorbing materials. J. Mater. Chem. A **2**, 735–744 (2014)

28. J. Yan, Y. Huang, Y.H. Yan, L. Ding, P.B. Liu, High-performance electromagnetic wave absorbers based on two kinds of nickel-based MOF-derived Ni@C microspheres. ACS Appl. Mater. Interface **11**, 40781–40792 (2019)

29. P.B. Liu, Y. Huang, X. Zhang, Superparamagnetic NiFe₂O₄ particles on poly (3,4-ethylenedioxythiophene)-graphene: synthesis, characterization and their excellent microwave absorption properties. Compos. Sci. Technol. **95**, 107–113 (2014)

30. J. Wei, Z. Zang, Y. Zhang, M. Wang, J. Du, X. Tang, Enhanced performance of light-controlled conductive switching in hybrid cuprous oxide/reduced graphene oxide (Cu₂O/rGO) nanocomposites. Opt. Lett. **42**, 911–914 (2017)

31. X. Zhao, W. Wang, Y.J. Zhang, S. Wu, F. Li, J.P. Liu, Synthesis and characterization of gadolinium doped cobalt ferrite nanoparticles with enhanced adsorption capability for Congo Red. Chem. Eng. J. **250**, 164–174 (2014)

32. K. Cai, W. Shen, B. Ren, J. He, S. Wu, W. Wang, A phytic acid modified CoFe₂O₄ magnetic adsorbent with controllable morphology, excellent selective adsorption for dyes and ultra-strong adsorption ability for metal ions. Chem. Eng. J. **330**, 936–946 (2017)

33. Y.F. Pan, G.S. Wang, Y.H. Yue, Fabrication of Fe₃O₄@SiO₂@RGO nanocomposites and their excellent absorption properties with low filler content. RSC Adv. **5**, 71718–71723 (2015)

34. J.J. Dong, Y. Lin, H.W. Zong, H.B. Yang, Hierarchical LiFe₅O₈@PPy core-shell nanocomposites as electrode materials for supercapacitors. Appl. Surf. Sci. **470**, 1043–1052 (2019)

35. H. Lv, Y. Guo, G. Wu, G. Ji, Y. Zhao, Z.J. Xu, Interface polarization strategy to solve electromagnetic wave interference issue. ACS Appl. Mater. Interface **9**, 5660–5668 (2017)

36. G. Wang, Z. Gao, S. Tang, C. Chen, F. Duan, S. Zhao, S. Lin, Y. Feng, L. Zhou, Y. Qin, Microwave absorption properties of carbon nanocoils coated with highly controlled magnetic materials by atomic layer deposition. ACS Nano **6**, 11009–11017 (2012)

37. X. Liu, Y. Chen, X. Cui, M. Zeng, R. Yu, G.S. Wang, Flexible nanocomposites with enhanced microwave absorption properties based on Fe₃O₄/SiO₂ nanorods and polyvinylidene fluoride. J. Mater. Chem. A **3**, 12197–12204 (2015)

38. J. Ma, M. Zhan, K. Wang, Ultralightweight silver nanowires hybrid polyimide composite foams for high-performance electromagnetic interference shielding. ACS Appl. Mater. Interface **7**, 563–576 (2015)

39. Y. Du, W. Liu, R. Qiang, Y. Wang, X. Han, J. Ma, P. Xu, Shell thickness-dependent microwave absorption of core-shell Fe₃O₄@C composites. ACS Appl. Mater. Interface **6**, 12997–13006 (2014)

40. Q. Liu, Q. Cao, X. Zhao, H. Bi, C. Wang, D.S. Wu, R. Che, Insights into size-dominant magnetic microwave absorption properties of CoNi microflowers via off-axis electron holography. ACS Appl. Mater. Interface **7**, 4233–4240 (2015)

41. C. Luo, W. Duan, X. Yin, J. Kong, Microwave-absorbing polymer-derived ceramics from cobalt-coordinated poly-(dimethylsilylene) diacetylenes. J. Phys. Chem. C **120**, 18721–18732 (2016)

42. J.T. Feng, Y.H. Hou, Y.C. Wang, L.C. Li, Synthesis of hierarchical ZnFe₂O₄@SiO₂@RGO core-shell microspheres for enhanced electromagnetic wave absorption. ACS Appl. Mater. Interface **9**, 14103–14111 (2017)

43. H.B. Yang, P.F. Liu, F. Yan, Y. Lin, T. Wang, A novel lead-free ceramic with layered structure for high energy storage applications. J. Alloy Compd. **773**, 244–249 (2019)

44. X.Y. Liu, H.B. Yang, F. Yan, Y. Qin, Y. Lin, T. Wang, Enhanced energy storage properties of BaTiO₃-

$Bi_{0.5}Na_{0.5}TiO_3$ lead-free ceramics modified by $SrY_{0.5}Nb_{0.5}O_3$. J. Alloy Compd. **778**, 97–104 (2019)

45. H.B. Yang, F. Yan, Y. Lin, T. Wang, F. Wang, Y.L. Wang, L.N. Guo, W.D. Tai, H. Wei, Lead-free $BaTiO_3$-$Bi_{0.5}Na_{0.5}TiO_3$-$Na_{0.73}Bi_{0.09}NbO_3$ relaxor ferroelectric ceramics for high energy storage. J. Eur. Ceram. Soc. **37**, 3303–3311 (2017)

46. D. Li, Y. Lin, M. Zhang, H.B. Yang, Achieved ultrahigh energy storage properties and outstanding charge-discharge performances in $(Na_{0.5}Bi_{0.5})_{0.7}Sr_{0.3}TiO_3$-based ceramics by introducing a linear additive. Chem. Eng. J. (2020). DOI:https://doi.org/10.1016/j.cej.2019.123729

47. Y. Lin, D. Li, M. Zhang, H.B. Yang, $(Na_{0.5}Bi_{0.5})_{0.7}Sr_{0.3}TiO_3$ modified by $Bi(Mg_{2/3}Nb_{1/3})O_3$ ceramics with high energy-storage properties and ultrafast discharge rate. J. Mater. Chem. C **8**, 2258–2264 (2020)

48. W.L. Song, M.S. Cao, L.Z. Fan, M.M. Lu, Y. Li, C.Y. Wang, H.F. Ju, Highly ordered porous carbon/wax composites for effective electromagnetic attenuation and shielding. Carbon **77**, 130–142 (2014)

49. B. Zhao, G. Shao, B.B. Fan, W.Y. Zhao, S.B. Zhang, K.K. Guan, R. Zhang, In situ synthesis of novel urchin-like ZnS/Ni_3S_2@Ni composite with a core-shell structure for efficient electromagnetic absorption. J Mater. Chem. C **3**, 10862–10869 (2015)

50. L. Wang, B. Wen, X.Y. Bai, C. Liu, H.B. Yang, Facile and green approach to the synthesis of zeoliticimidazolate framework nanosheet-derived 2D Co/C composites for a lightweight and highly efficient microwave absorber. J Colloid Interface Sci. **540**, 30–38 (2019)

51. Y. Lin, J.J. Dong, H.W. Zong, B. Wen, H.B. Yang, Synthesis, characterization, and electromagnetic wave absorption properties of composites of reduced graphene oxide with porous $LiFe_5O_8$ microspheres. ACS Sustain. Chem. Eng. **6**, 10011–10020 (2018)

52. Y. Qiu, Y. Lin, H.B. Yang, L. Wang, M.Q. Wang, B. Wen, Hollow Ni/C microspheres derived from Ni-metal organic framework for electromagnetic wave absorption. Chem. Eng. J. **383**, 123207 (2020)

53. H.R. Yuan, F. Yan, C.Y. Li, C.L. Zhu, X.T. Zhang, Y.J. Chen, Nickel nanoparticle encapsulated in few-layer nitrogen-doped graphene supported by nitrogen-doped graphite sheets as a high-performance electromagnetic wave absorbing material. ACS Appl. Mater. Interface **10**, 1399–1407 (2018)

54. P.J. Liu, Z.J. Yao, J.T. Zhou, Z.H. Yang, L.B. Kong, Small magnetic Co-doped NiZn ferrite/grapheme nanocomposites and their dual-region microwave absorption performance. J Mater. Chem. C **4**, 9738–9749 (2016)

55. Y. Liu, Z. Chen, Y. Zhang, R. Feng, X. Chen, C.X. Xiong, L.J. Dong, Broadband and lightweight microwave absorber constructed by in situ growth of hierarchical $CoFe_2O_4/$

56. T. Zhua, S.C. Chang, Y.F. Song, M. Lahoubic, W. Wang, PVP-encapsulated $CoFe_2O_4$/rGO composites with controllable electromagnetic wave absorption performance. Chem. Eng. J. **373**, 755–766 (2019)

57. P. Liu, V.M.H. Ng, Z. Yao, J. Zhou, Y. Lei, Z. Yang, H. Lv, L. Kong, Facile synthesis and hierarchical assembly of flower-like NiO structures with enhanced dielectric and microwave absorption properties. ACS Appl. Mater. Interface **9**, 16404–16414 (2017)

58. G.M. Rutter, J.N. Crain, N.P. Guisinger, T. Li, P.N. First, J.A. Stroscio, Scattering and interference in epitaxial graphene. Science **317**, 219–222 (2007)

59. X. Sun, J.P. He, G.X. Li, J. Tang, T. Wang, Y.X. Guo, H.R. Xue, Laminated magnetic graphene with enhanced electromagnetic wave absorption properties. J. Mater. Chem. C **1**, 765–777 (2013)

60. M. Zong, Y. Huang, N. Zhang, H.W. Wu, Influence of (RGO)/(ferrite) ratios and graphene reduction degree on microwave absorption properties of graphene composites. J. Alloy Compd. **644**, 491–501 (2015)

61. L. Kong, X. Yin, Y. Zhang, X. Yuan, Q. Li, F. Ye, L. Cheng, L. Zhang, Electromagnetic wave absorption properties of reduced graphene oxide modified by maghemite colloidal nanoparticle clusters. J. Phys. Chem. C **117**, 19701–19711 (2013)

62. M. Han, X. Yin, L. Kong, M. Li, W. Duan, L. Zhang, L. Cheng, Graphene-wrapped ZnO hollow spheres with enhanced electromagnetic wave absorption properties. J. Mater. Chem. A **2**, 16403–16409 (2014)

63. H. Wu, H.F. Li, G.B. Sun, S.L. Ma, X.J. Yang, Synthesis, characterization and electromagnetic performance of nanocomposites of graphene with α-$LiFeO_2$ and β-$LiFe_5O_8$. J. Phys. Chem. C **3**, 5457–5466 (2015)

64. Z. Yang, Y. Wan, G. Xiong, D. Li, Q. Li, C. Ma, R. Guo, H. Luo, Facile synthesis of $ZnFe_2O_4$/reduced graphene oxide nanohybrids for enhanced microwave absorption properties. Mater. Res. Bull. **61**, 292–297 (2015)

65. D. Moitra, S. Dhole, B.K. Ghosh, M. Chandel, R.K. Jani, M.K. Patra, S.R. Vadera, N.N. Ghosh, Synthesis and microwave absorption properties of $BiFeO_3$ nanowire-rGO nanocomposite and first-principles calculations for insight of electromagnetic properties and electronic structures. J. Phys. Chem. C **121**, 21290–21304 (2017)

66. D. Moitra, B. Ghosh, M. Chandel, R. Jani, M. Patra, S. Vadera, N. Ghosh, Synthesis of a $Ni_{0.8}Zn_{0.2}Fe_2O_4$-rGO nanocomposite: an excellent magnetically separable catalyst for dye degradation and microwave absorber. RSC Adv. **6**, 14090–14096 (2016)

67. P.B. Liu, Y. Huang, X. Sun, Excellent electromagnetic absorption properties of poly (3,4-ethylenedioxythiophene)-reduced graphene oxide-Co$_3$O$_4$ composites prepared by a hydrothermal method. ACS Appl. Mater. Interface **5**, 12355–12360 (2013)

68. Y. Wang, Y.B. Chen, X.M. Wu, W.Z. Zhang, C.Y. Luo, J.H. Li, Fabrication of MoS$_2$-graphene modified with Fe$_3$O$_4$ particles and its enhanced microwave absorption performance. Adv. Powder Technol. **29**, 744–750 (2018)

69. D.P. Sun, Q. Zou, Y.P. Wang, Y.J. Wang, W. Jiang, F.S. Li, Controllable synthesis of porous Fe$_3$O$_4$@ZnO sphere decorated graphene for extraordinary electromagnetic wave absorption. Nanoscale **6**, 6557–6562 (2014)

Publisher's Note Springer Nature remains neutral with regard to jurisdictional claims in published maps and institutional affiliations.